Journal of Microscopy

Journal of Microscopy, Vol. 251, Issue 1 2013, pp. 19–26 doi: 10.1111/jmi.12038
Received 15 November 2012; accepted 14 March 2013

Measuring absolute nanoparticle number concentrations from particle count time series

M. RÖDING*, H. DESCHOUT†,‡, K. BRAECKMANS†,‡ & M. RUDEMO*

**Department of Mathematical Statistics, Chalmers University of Technology and Gothenburg University, Gothenburg, Sweden*

†Laboratory of General Biochemistry and Physical Pharmacy, Ghent University, Ghent, Belgium

‡Center for Nano– and Biophotonics, Ghent University, Ghent, Belgium

Key words. Concentration measurements, fluorescence microscopy, single-particle methods, Smoluchowski process.

Summary

Single-particle microscopy is important for characterization of nanoparticulate matter for which accurate concentration measurements are crucial. We introduce a method for estimating absolute number concentrations in nanoparticle dispersions based on a fluctuating time series of particle counts, known as a Smoluchowski process. Thus, unambiguous tracking of particles is not required and identification of single particles is sufficient. However, the diffusion coefficient of the particles must be estimated separately. The proposed method does not require precalibration of the detection region volume, as this can be estimated directly from the observations. We evaluate the method in a simulation study and on experimental data from a series of dilutions of 0.2- and 0.5-μm polymer nanospheres in water, obtaining very good agreement with reference values.

Introduction

There has been a growing interest in observing and understanding single particles and single molecules lately, and in particular functional nanoparticles. Applications include using nanoparticles for drug delivery (Remaut *et al.*, 2007), in biomedical imaging (Nune *et al.*, 2009) and as biomarkers (Chironi *et al.*, 2009; Doevre *et al.*, 2009). A thorough understanding of the fundamental interactions of nanomaterials with biological systems, at the single particle and single molecule level, will without doubt play a central role in the future nanobioscience field (Deniz *et al.*, 2008; Nel *et al.*, 2009; Soenen *et al.*, 2009). The search for detection and characterization methods for nanoparticulate matter, particularly using single-particle or single-molecule methods, has received a lot of attention (Gaumet *et al.*, 2008; Morris *et al.*, 2009; Vysotskii *et al.*, 2009), especially concerning nanoparticles in biological materials such as blood, tissues or cells (Braeckmans *et al.*, 2010a,b,c; Montes-Burgos *et al.*, 2010; van Gaal *et al.*, 2009). Relevant parameters are size (distribution), shape, surface properties and concentration (Decuzzi *et al.*, 2010; Gaumet *et al.*, 2008; Koide *et al.*, 2008; Lundqvist *et al.*, 2008).

A widely used approach is to use fluorescence microscopy to perform particle tracking. However, particle tracking is not the only means of extracting information using fluorescence microscopy. Indeed, information from a particulate system can be extracted by studying fluctuations (Petrášek & Schwille, 2009). In this work, we study how to use fluctuations of *Smoluchowski processes* to estimate absolute particle number concentration. By a Smoluchowski process we mean a time series of particle counts, named in honour of Polish physicist M. von Smoluchowski who developed an alternative to Einstein's description of Brownian motion. For early theoretical treatments and experimental verifications of Smoluchowski's original model, see Chandrasekhar (1943), Svedberg & Inouye (1911), von Smoluchowski (1906, 1916), Westgren (1916). The perhaps most remarkable application of Smoluchowski's theory is the classical experiment by Svedberg & Inouye (1911) in which Avogadro's constant, a number in the order of 10^{23}, was estimated from a time series of 517 particle counts ranging from 0 to 6. The nature of a particular Smoluchowski process depends on the behaviour of the particles, i.e. diffusive or nondiffusive, diffusion coefficient (monodisperse or polydisperse sample), the particle concentration, but also on the conditions under which the particles are observed, i.e. the volume and shape of the detection region. An example of an experimentally observed Smoluchowski process formed by counting diffusing liposomes in whole blood is shown in Figure 1.

Fluorescence microscopy is of great interest for in particular (undiluted) biological fluids (Braeckmans *et al.*, 2010a).

Correspondence to: Magnus Röding, Chalmers University of Technology, Mathematical Sciences, 41296 Gothenburg, Sweden. Tel: +46317724992; e-mail: roding@chalmers.se

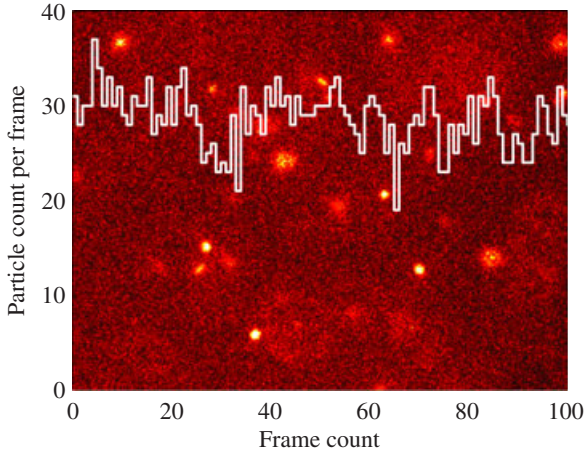

Fig. 1. An example of an experimentally observed Smoluchowski process formed by counting diffusing liposomes in whole blood, superimposed over a sample frame from the raw image data.

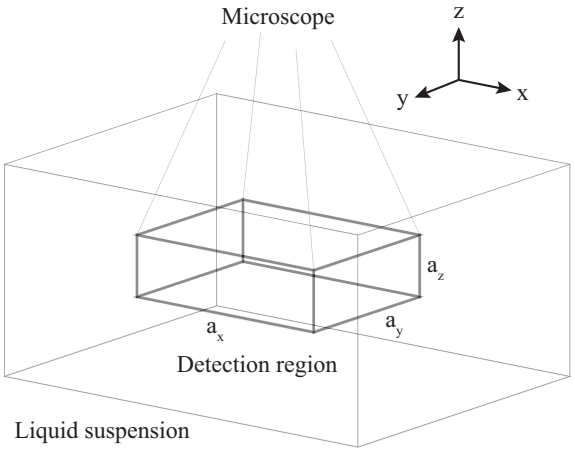

Fig. 2. The experimental setup. Centred in a liquid suspension is a detection region. The lateral sizes $2a_x$ and $2a_y$ of the detection region are known, but the axial size (detection depth) $2a_z$ is not directly observable. (Figure not to scale.)

We have recently demonstrated that an absolute number concentration of nanoparticles can be estimated from single-particle tracking experiments using a framework that is independent of prior calibration of the detection region volume, by using a statistical model for the distribution of trajectory lengths observed in the experimental data (Röding *et al.*, 2011). This is of great practical relevance since the detection region is dependent on experimental parameters, such as illumination strength, particle brightness and image processing. One drawback of this previous method is that single particles have to be tracked, thereby limiting the method to rather small concentrations.

In the present alternative approach, we model and observe Smoluchowski processes depending on diffusion coefficient, detection region volume and particle number concentration. A benefit of this new approach is that single particles do not need to be tracked. We use this model to estimate first the detection region volume and then the absolute number concentration of nanoparticles. We consider an approximate Markov model for the Smoluchowski process. The estimated concentrations are validated on both simulated and experimental data. In the latter case, the estimated concentrations are compared to reference measurements.

The text is organized as follows. First, the problem description and the theoretical modelling and estimation are covered. Secondly, a simulation study is performed. Finally, experimental data are analyzed.

Theory and methods

Concentration measurements

Consider a suspension of particles in a fluid, in the centre of which we have a rectangular (three-dimensional) detection region. The lateral sizes $2a_x$ and $2a_y$ of the detection region are determined by the field of view of the microscope (and can be precisely measured by means of, e.g. a calibration grid), and the axial size $2a_z$ (perpendicular to the focal plane) is defined by what can be referred to as the *detection depth*, the distance from the nearest to the most distant detectable particles [equivalent to the *tracking depth* in Röding *et al.*, (2011), see Fig. 2]. By assumption, we do not detect the axial coordinates of the particles in the detection region and consequently the detection depth is unknown, depending on experimental parameters, such as illumination strength, particle brightness and image processing settings (since these parameters have an impact on how far away from the focal plane a particle will be detected). Assume that the particles diffuse freely within the liquid suspension. The diffusive motion of each particle is described by a Brownian motion $B(t)$ with $t \geq 0$ characterized by the mean squared deviation property

$$\mathrm{E}[\|B(t) - B(0)\|^2] = 2\mathcal{N}Dt, \tag{1}$$

where $\mathcal{N}$ is the number of dimensions (Berg, 1993) (physically, $\mathcal{N} = 3$, but we only have observations for $\mathcal{N} = 2$), and D is the diffusion coefficient. By assumption, D can be estimated separately.

Assume we acquire discrete observation of a Smoluchowski process $X(t)$ (a series of particle counts as a function of time) in diffusion equilibrium at regular time intervals with time lapse Δt (see Fig. 3).

Denote the nth observation by X_n (the number of particles in the nth frame). From one observation to the next, a number of particles have entered and a number of particles have left the detection region. Thus

$$X_{n+1} = X_n - O_n + I_n, \tag{2}$$

where O_n is the number of particles (out of the X_n particles initially present) exiting the detection region between the

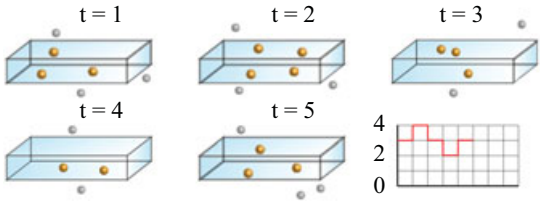

Fig. 3. Illustration of the formation of a Smoluchowski process. Diffusing particles reside both inside (yellow) and outside (grey, dim) the detection region. Particles are moving in and out of the detection region and the number of detected particles is fluctuating, forming a random time series. (Figure not to scale.)

observations X_n and X_{n+1}, and I_n is the number of particles entering the detection region between these observations. Without any additional prior knowledge, a reasonable assumption is that the X_n particles in frame n are uniformly distributed within the detection region. Hence, given $X_n = i$, we assume that O_n follows a binomial distribution with index i and parameter μ, i.e. $O_n|X_n = i \sim \mathrm{Bin}(i, \mu)$. Furthermore, we assume that I_n follows a Poisson distribution with parameter λ, $I_n \sim \mathrm{Po}(\lambda)$. Based on these assumptions, we approximate the particle counts $\{X_n\}$ with a Markov model, for which the transition probabilities $p_{ij} = P(X_{n+1} = j|X_n = i)$ are

$$p_{ij}(\lambda, \mu) = e^{-\lambda} \sum_{k=\max(0,\, j-i)}^{j} \frac{\lambda^k}{k!} \binom{i}{i-j+k} \times \mu^{i-j+k}(1-\mu)^{j-k} \tag{3}$$

for all $i \geq 0$ and $j \geq 0$ (see Appendix A). The stationary distribution of this Markov chain is a Poisson distribution with parameter λ/μ (see Appendix C), i.e.

$$P(X_n = k) = \pi_k = \frac{(\lambda/\mu)^k e^{-\lambda/\mu}}{k!} \tag{4}$$

for all $k \geq 0$ and all n. (In fact, the Markov assumption is an approximation (which is equivalent to the approximation that the trajectory length distribution in Röding *et al.* (2011) is a geometric distribution), as noted already by Patil (1957).)

The joint distribution of particle counts $X_1, \ldots, X_N$ can, given the Markov assumption, be written

$$P(X_1 = x_1, \ldots, X_N = x_N) = P(X_1 = x_1) \times \prod_{k=2}^{N} P(X_k = x_k|X_{k-1} = x_{k-1}). \tag{5}$$

Considering a realization $x_1, \ldots, x_N$, we obtain the log-likelihood function

$$l(\lambda, \mu) = l(\lambda, \mu|x_1, \ldots, x_N) = \log \frac{(\lambda/\mu)^{x_1} e^{-\lambda/\mu}}{x_1!} + \sum_{i,j} N_{ij} \log p_{ij}(\lambda, \mu), \tag{6}$$

where N_{ij} is the number of transitions from state i to j. This generalizes without effort to the case where data are acquired from several independent videos (rather than from frames of a single video), by summation of log-likelihood functions like Eq. (6). We obtain the maximum likelihood estimates $\hat{\lambda}$ and $\hat{\mu}$ by maximizing the log-likelihood.

Now, let ϕ denote the standard normal density and Φ the standard normal cumulative distribution function. Since μ can be interpreted as the probability

$$\begin{aligned} P_{\mathrm{exit}}(a_z) = 1 - \frac{(2D\Delta t)^{3/2}}{8a_x a_y a_z} & \times \left\{ \frac{2a_x}{\sqrt{2D\Delta t}} \left[2\Phi\left(\frac{2a_x}{\sqrt{2D\Delta t}} \right) - 1 \right] + 2\phi\left(\frac{2a_x}{\sqrt{2D\Delta t}} \right) - 2\phi(0) \right\} \\ & \times \left\{ \frac{2a_y}{\sqrt{2D\Delta t}} \left[2\Phi\left(\frac{2a_y}{\sqrt{2D\Delta t}} \right) - 1 \right] + 2\phi\left(\frac{2a_y}{\sqrt{2D\Delta t}} \right) - 2\phi(0) \right\} \\ & \times \left\{ \frac{2a_z}{\sqrt{2D\Delta t}} \left[2\Phi\left(\frac{2a_z}{\sqrt{2D\Delta t}} \right) - 1 \right] + 2\phi\left(\frac{2a_z}{\sqrt{2D\Delta t}} \right) - 2\phi(0) \right\}, \end{aligned} \tag{7}$$

that a uniformly distributed particle exits the detection region (see Appendix B), we can obtain an estimate $\hat{a}_z$ of the detection depth parameter a_z from $P_{\mathrm{exit}}(a_z) = \mu$ (recall that a_x and a_y are simply obtained by calibration of the microscope using a grid and thus known, so that a_z is the only unknown here). (By the invariance property, $\hat{a}_z$ is also a maximum likelihood estimate (Pawitan, 2001).) To estimate the number concentration C, we divide the mean number of detected particles per frame by the detection region volume. The mean number of detected particles can be estimated by $\hat{\lambda}/\hat{\mu}$ (recall that the mean value of the stationary Poisson-distributed Markov chain is λ/μ). We obtain

$$\hat{C} = \frac{\hat{\lambda}/\hat{\mu}}{8a_x a_y \hat{a}_z 10^{-12}} \text{particles mL}^{-1}, \tag{8}$$

where $\hat{\lambda}$ and $\hat{\mu}$ are obtained by maximization of the log-likelihood in Eq. (6), and $\hat{a}_z$ is obtained from $\hat{\mu}$ through Eq. (7). The length unit is μm. (Once again by the invariance property, $\hat{C}$ is a maximum likelihood estimate.) The method is implemented in Matlab (Mathworks, Natick, MA, U.S.A.) (see Supporting Information).

Bootstrap confidence intervals

There are many sources of variability in the final concentration estimate $\hat{C}$. In addition to the inherent finite-sample variability of the estimate, the Markov model approximation

and noise distortion (false negatives and false positives originating from the image processing algorithm for detecting individual particles) contribute to the variability of $\hat{C}$. Since all of this will inevitably be part of the concentration estimate in practical applications, the corresponding variability must be accounted for. We use here the nonparametric bootstrap (Efron & Tibshirani, 1993) on the 'video level'. Given a data set $\{x^{(1)}, \ldots, x^{(M)}\}$, where $x^{(m)}$ is the process observed in the mth video, we extract a bootstrap sample by sampling from the set of M videos *with replacement*, yielding a bootstrap data set $\{x^{(1),b}, \ldots, x^{(M),b}\}$, where $b = 1, \ldots, B$ where B is the number of bootstrap data sets. For each bootstrap sample, an estimate $\hat{C}$ is computed. This yields an approximation of the true distribution of $\hat{C}$, from which standard errors can be estimated.

Simulation study

We performed a simulation study to validate the model for estimating the concentration. We let noninteracting point particles diffuse in three dimensions in a virtual liquid suspension with periodic boundary conditions (hence, the concentration is constant, with no net flux). A predetermined number of particles were initially placed randomly in the liquid suspension (all three coordinates being uniformly distributed). For each time increment Δt, particles performed a random walk in each of the three directions, independent of the other directions, with normally distributed increments of mean zero and variance $2D\Delta t$, and the particles in the virtual detection region were counted. We let the lateral size of the detection region be 40 μm (roughly similar to the parameters of the experimental data, see Appendix D) in both directions. We let the liquid suspension be 100 μm in all three directions. The simulations were run in Matlab (Mathworks, Natick, MA, U.S.A.) (see Supporting Information).

We validated the estimate of the concentration on simulated data sets resembling the experimentally obtained data sets. We used three different diffusion coefficients, $D = 1$, $D = 2$ and $D = 5$ μm^2 s^{-1} (corresponding roughly to the range 0.1–0.5 μm in diameter for particles diffusing in water), and values of a_z varying between 0.1 and 2 μm in increments of 0.1 μm (a value of $a_z = 1$ μm corresponds approximately to the experimental conditions). A total of 30 video sequences, each of length 10 s (250 frames, $\Delta t = 40$ ms), were simulated in each run. The true concentration of particles was $C = 10^9$ particles mL^{-1} throughout. The mean estimates as computed from 10^6 simulations for each data point (each combination of a_z and D) are presented in Figure 4. We see that the bias decreases as a_z increases, although the bias at $a_z = 0.1$ μm is small already ($\leq$2%). In addition, it is found that using 50 or more bootstrap samples, the standard error of both the detection depth parameter and the concentration estimate could be estimated quite precisely (not shown). With an additional simulation study it is found that a polydispersity of less than

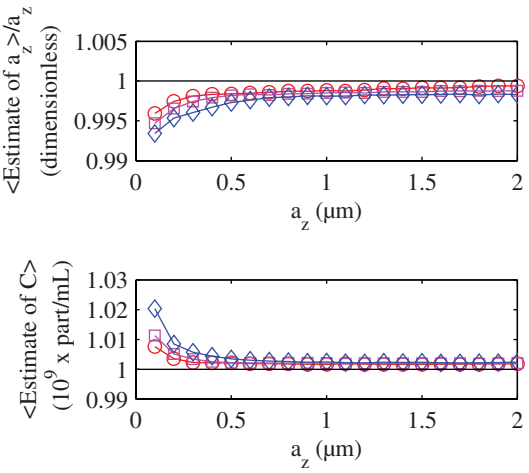

Fig. 4. Simulation study of the detection depth parameter (upper) and concentration estimate (lower). For $D = 1$ μm^2 s^{-1} (red, circles), $D = 2$ μm^2 s^{-1} (magenta, squares) and $D = 5$ μm^2 s^{-1} (blue, diamonds), the mean estimates of a_z (divided by the true value of a_z) and C are shown as a function of the true value of a_z. The mean estimates are computed from 10^6 simulations for each data point (each combination of a_z and D). The true concentration of particles was $C = 10^9$ particles mL^{-1}.

50% yields a less than 2% additional bias on the results (not shown).

Experimental results

To experimentally verify the theory, experiments were carried out on dispersions of fluorescent polymer nanospheres using a custom-built laser widefield epifluorescence microscope setup. Using custom developed software, the movies are analyzed to identify individual particles in each frame of the movie (Braeckmans *et al.*, 2010a) (see Appendix D).

Two different sizes of 'dragon green' (excitation 480 nm, emission 520 nm) fluorescent polymer nanospheres (Bangs Laboratories, Fishers, IN, U.S.A.) were studied. First, a water dispersion of 0.2 μm particles was diluted to a factor of 1900, 2400, 3400, 5800 and 14 800. Single-particle experiments were carried out on each dilution and the concentrations were estimated. The theoretical number concentration in particles mL^{-1} of the stock solution can be estimated using

$$C_{\text{theoretical}} = \frac{6 \times 10^{10} \times S\rho_L}{\pi \rho_S d^3}, \qquad (9)$$

where $S = 1$ is the weight percentage of solids, with a relative standard deviation of 5%, $\rho_L = 1.00$ g cm^{-3} is the density of the suspension, $\rho_S = 1.05$ g cm^{-3} is the density of the solid particles (all values according to manufacturer), and using dynamic light scattering the mean diameter of the particles was found to be $d = 0.207$ μm with a standard deviation of 0.008 μm (in correspondence with manufacturer results for that particular batch of nanospheres). Second, a water

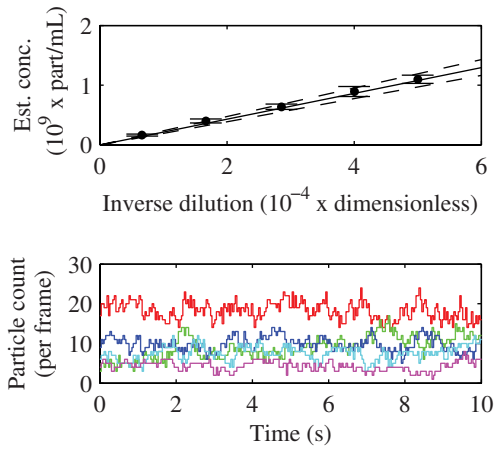

Fig. 5. Estimated concentrations for different dilutions of 0.2 μm particles with estimated 95% confidence intervals ('inverse dilution' is a 'relative concentration'). The concentration as estimated from the stock solution concentration (solid line) with estimated 95% confidence intervals (dashed lines) is shown (upper). Also, typical examples of the underlying Smoluchowski processes are shown, with colours red/green/blue/cyan/magenta in order of decreasing concentration (lower).

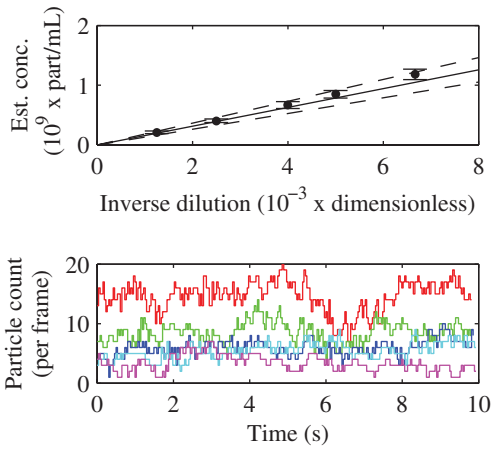

Fig. 6. Estimated concentrations for different dilutions of 0.5 μm particles with estimated 95% confidence intervals ('inverse dilution' is a 'relative concentration'). The concentration as estimated from the stock solution concentration (solid line) with estimated 95% confidence intervals (dashed lines) is shown (upper). Also, typical examples of the underlying Smoluchowski processes are shown, with colours red/green/blue/cyan/magenta in order of decreasing concentration (lower).

dispersion of 0.5 μm particles was diluted to a factor of 140, 190, 240, 380 and 750. Using dynamic light scattering, the mean diameter of the particles was found to be $d = 0.497$ μm with a standard deviation of 0.009 μm (in correspondence with manufacturer results for that particular batch of nanospheres). Using the standard propagation of error equation, theoretical number concentrations with standard deviations can be found for all dilutions, and compared with the results from our method.

As is clear from the results in Figures 5 and 6, an excellent agreement was found between the theoretically and experimentally obtained concentration values. All values are within the confidence intervals for the reference values. Note that we used the diffusion coefficients D=2.32 μm^2 s^{-1} for 0.2 μm particles and D=0.98 μm^2 s^{-1} for 0.5 μm particles (obtainable by, e.g. dynamic light scattering measurements). We would like to stress the fact that this result is obtained without any precalibration of the detection region volume, and that the detection region volume is estimated independently for each dilution. See Supporting Information for experimental data sets.

Discussion and conclusion

In this work, we have derived and validated a theoretical model for particle count fluctuations, the so-called Smoluchowski process, in a single-particle imaging experiment and demonstrated its use for estimation of the particle detection region volume and the absolute number concentration of nanoparticles in a dispersion. Confidence intervals for both the detection depth parameter and the absolute concentration, giving accurate accounts of the uncertainty of the estimates, can also be acquired. The method was experimentally validated by estimating the number concentration of different dilutions of 0.2- and 0.5-μm fluorescent carboxylated polymer nanospheres. We found a very good agreement between our concentration estimates and the reference measurements. In conclusion, we have demonstrated the validity and usefulness of this approach for accurate, absolute particle number concentration measurements, using a model which takes the inherent variability of particle detection due to image processing and other conditions into account. We believe this to be highly useful for characterization of nanoparticles in many situations, in particular in (even undiluted) biological fluids where single-particle techniques have shown much promise (even though one obvious drawback of the this work is the required separate estimation of the diffusion coefficient), especially for high concentrations where unambiguously determining single particle trajectories becomes problematic. Further work might include a performance comparison between this method and Fluorescence Correlation Spectroscopy and Image Correlation Spectroscopy for different particle sizes, concentrations and polydispersity. It might also include model extensions to the cases of directed motion, anomalous diffusion and polydispersity, as well as investigations on the impact of particle detection accuracy with regard to e.g. photobleaching on the result.

Acknowledgements

Acknowledgements go to Aila Särkkä for careful reading of the manuscript. Some of the computations were performed

on C3SE (Chalmers Centre for Computational Science and Engineering) resources. Hendrik Deschout is a doctoral fellow of the Institute for the Promotion of Innovation through Science and Technology in Flanders (IWT), Belgium. This work has been carried out with financial support from the Swedish Foundation for Strategic Research (SSF) through Gothenburg Mathematical Modelling Centre (GMMC), the Swedish Governmental Agency for Innovation Systems (VINNOVA) through SuMo Biomaterials Centre, Stiftelsen Längmanska Kulturfonden, Friends of Chalmers Foundation and the Funds for Scientific Research, Flanders (project G.0197.11).

References

Berg, H.C. (1993) *Random Walks in Biology*. Princeton University Press, Princeton, NJ.

Braeckmans, K., Buyens, K., Bouquet, W., *et al.* (2010a) Sizing nanomatter in biological fluids by fluorescence single particle tracking. *Nano Lett.* **10,** 4435–4442.

Braeckmans, K., Buyens, K., Naeye, B., *et al.* (2010b) Advanced fluorescence microscopy methods illuminate the transfection pathway of nucleic acid nanoparticles. *J. Control. Release* **148,** 69–74.

Braeckmans, K., Vercauteren, D., Demeester, J. & Smedt, S.D. (2010c) Single particle tracking. *Nanoscopy Multidimensional Optical Fluorescence Microscopy* (ed. by E. Diaspro). Chapman and Hall, Boca Raton, FL.

Chandrasekhar, S. (1943) Stochastic problems in physics and astronomy. *Rev. Mod. Phys.* **15**(1), 1–89.

Chironi, G., Boulanger, C., Simon, A., Dignat-George, F., Freyssinet, J. & Tedgui, A. (2009) Endothelial microparticles in diseases. *Cell Tissue Res.* **335,** 143–151.

Decuzzi, P., Godin, B., Tanaka, T., Lee, S.Y., Chiappini, C., Liu, X. & Ferrari, M. (2010) Size and shape effects in the biodistribution of intravascularly injected particles. *J. Control. Release* **141,** 320–327.

Deniz, A., Mukhopadhyay, S. & Lemke, E. (2008) Single-molecule biophysics: at the interface of biology, physics and chemistry. *J. R. Soc. Inter.* **5,** 15–45.

Doevre, L., Plawinski, L., Toti, F. & Anglés-Cano, E. (2009) Cell-derived microparticles: a new challange in neuroscience. *Cell Tissue Res.* **335,** 143–151.

Efron, B. & Tibshirani, R. (1993) *An Introduction to the Bootstrap*. Chapman and Hall, Boca Raton, FL.

van Gaal, E., Spierenburg, G., Hennink, W., Crommelin, D. & Mastrobattista, E. (2009) Flow cytometry for rapid size determination and sorting of nucleic acid containing nanoparticles in biological fluids. *J. Control. Release.* **141,** 328–338.

Gaumet, M., Vargas, A., Gurny, R. & Delie, F. (2008) Nanoparticles for drug delivery: the need for precision in reporting particle size parameters. *Eur. J. Pharm. Biopharm.* **69,** 1–9.

Grimmett, G. & Stirzaker, D. (2001) *Probability and Random Processes*, 3rd edition. Oxford University Press, Oxford, UK.

Koide, H., Asai, T., Urakami, K.H.T., *et al.* (2008) Particle size-dependent triggering of accelerated blood clearance phenomenon. *Int. J. Pharm.* **362,** 197–200.

Lundqvist, M., Stigler, J., Elia, G., Lynch, I., Cedervall, T. & Dawson, K. (2008) Nanoparticle size and surface properties determine the protein corona with possible implications for biological impacts. *Proc. Natl. Acad. Sci.* **105,** 14265–14270.

Montes-Burgos, I., Walczyk, D., Hole, P., Smith, J., Lynch, I. & Dawson, K. (2010) Characterisation of nanoparticle size and state prior to nanotoxicological studies. *J. Nanopart. Res.* **12,** 47–53.

Morris, A., Watzky, M. & Finke, R. (2009) Protein aggregation kinetics, mechanism, and curve-fitting: a review of the literature. *Biochim. Biophys. Acta.* **1794,** 375–397.

Nel, A., Mädler, L., Velegol, D., *et al.* (2009) Understanding biophysicochemical interactions at the nano-bio interface. *Nature Mater.* **8,** 543–557.

Nune, S., Gunda, P., Thallapally, P., Lin, Y., Forrest, M. & Berkland, C. (2009) Nanoparticles for biomedical imaging. *Expert Opin. Drug Deliv.* **6,** 1175–1194.

Patil, V. (1957) The consistency and adequacy of the Poisson-Markoff model for density fluctuations. *Biometrika* **44,** 43–56.

Pawitan, Y. (2001) *In All Likelihood: Statistical Modelling and Inference Using Likelihood*. Oxford University Press, Oxford, UK.

Petrášek, Z. & Schwille, P. (2009) Fluctuations as a source of information in fluorescence microscopy. *J. R. Soc. Inter.* **6,** S15–S45.

Remaut, K., Sanders, N., Geest, B.D., Braeckmans, K., Demeester, J. & Smedt, S.D. (2007) Nucleic acid delivery: where material sciences and bio-sciences meet. *Mat. Sci. Eng. R.* **58,** 117–161.

Röding, M., Deschout, H., Braeckmans, K. & Rudemo, M. (2011) Measuring absolute number concentrations of nanoparticles using single-particle tracking. *Phys. Rev. E.* **84,** 031920.

Rothschild, L. (1953) A new method of measuring the activity of spermatozoa. *J. Exp. Biol.* **30,** 178–199.

Soenen, S., Vercauteren, D., Braeckmans, K., Noppe, W., Smedt, S.D. & Cuyper, M.D. (2009) Stable long-term intracellular labelling with fluorescently tagged cationic magnetoliposomes. *Chembiochem.* **10,** 257–267.

Svedberg, T. & Inouye, K. (1911) Eine neue Methode zur Prüfung der Gültigkeit des Boyle-Gay-Lussacschen Gesetzes für kolloide Lösungen (A novel method of proving the validity of the Boyle-Gay-Lussac law for colloidal dispersions). *Z. Phys. Chem.* **77,** 145–190.

Von Smoluchowski, M. (1906) Zur kinetischen Theorie der Brownschen Molekulärbewegung und der Suspensionen (On the kinetic theory of Brownian molecular motion and suspensions). *Ann. Phys. (Berlin)* **21,** 756–780.

Von Smoluchowski, M. (1916) Drei Vorträge über Diffusion, Brownsche Molekulärbewegung und Koagulation von Kolloidteilchen (Three lectures on diffusion, Brownian molecular motion and coagulation of colloidal particles). *Physik Z.* **17,** 557–571 and 587–599.

Vysotskii, V., Uryupina, O., Guselnikova, A. & Roldugin, V. (2009) On the feasibility of determining nanoparticle concentration by the dynamic light scattering method. *Colloid J.* **71,** 739–744.

Westgren, A. (1916) Die Veränderungsgeschwindigkeit der lokalen Teilchenkonzentration in kolloiden Systemen, I. (The change velocity of the local particle concentration in colloidal systems). *Ark. Mat. Astr. Fys.* **11,** 1–24.

Appendix A: Transition probabilities

Let the number of particles residing within the detection region at time $n\Delta t$ be $X_n \in \{0, 1, 2, \ldots\}$. We want to formulate a model for the number of particles X_{n+1} residing in the detection region at time $(n+1)\Delta t$. In principle, the number of particles entering the detection region in each time step follows a binomial distribution, but since at any given moment

the number of particles in the liquid suspension which are not residing within the detection region is large, we can approximate this binomial distribution with a Poisson distribution. Not conditioned on how long the particles have resided within the detection region, the number of particles exiting the detection region is binomially distributed. We can write

$$X_{n+1} = X_n + I_n - O_n, \tag{10}$$

where I_n is the number of particles entering the detection region in the time interval from $n\Delta t$ to $(n+1)\Delta t$ and is Poisson distributed with parameter λ. Hence, its probability distribution is

$$P(I_n = k|\lambda) = \frac{\lambda^k e^{-\lambda}}{k!}, \quad k \geq 0. \tag{11}$$

Moreover, O_n is the number of particles (out of the X_n particles) that exit the detection region between $n\Delta t$ and $(n+1)\Delta t$ and is, conditionally on $X_n = i$, binomially distributed with parameters i and μ, i.e.

$$P(O_n = k|i, \mu) = \binom{i}{k} \mu^k (1-\mu)^{i-k}, \quad 0 \leq k \leq i, \tag{12}$$

where

$$\binom{i}{k} = \frac{i!}{k!(i-k)!} \tag{13}$$

is the binomial coefficient. We assume now that $\{X_n\}$ is approximately a Markov chain with transition probabilities determined by Eq. (10) with O_n and I_n binomially and Poisson distributed as described earlier. This gives

$$\begin{aligned} p_{ij}(\lambda, \mu) &= P(X_{n+1} = j | X_n = i) \\ &= P(I_n - O_n = j - i) \\ &= \sum_{k=0}^{\infty} P(I_n = k) P(O_n = i - j + k) \end{aligned} \tag{14}$$

of which the terms obviously are nonzero if and only if $0 \leq i - j + k \leq i$ and $k \geq 0$; these two constraints can be summarized by $\max(0, j-i) \leq k \leq j$. We finally reach the result

$$\begin{aligned} p_{ij}(\lambda, \mu) = e^{-\lambda} &\sum_{k=\max(0, j-i)}^{j} \frac{\lambda^k}{k!} \\ &\times \binom{i}{i-j+k} \mu^{i-j+k} (1-\mu)^{j-k} \end{aligned} \tag{15}$$

for $i \geq 0$ and $j \geq 0$.

Appendix B: Probability of a uniformly distributed particle to exit the detection region

We compute the probability of a uniformly distributed particle to exit the detection region. Assume that the lateral sizes of the detection region are $2a_x$ and $2a_y$, respectively. Assume that the axial size is $2a_z$. Let ϕ denote the standard normal density and Φ the standard normal cumulative distribution function

$$\phi(z) = \frac{1}{\sqrt{2\pi}} e^{-\frac{1}{2}z^2} \quad \text{and} \quad \Phi(z) = \int_{-\infty}^{z} \phi(t) dt. \tag{16}$$

Assuming thermodynamic equilibrium, particles in the detection region are uniformly distributed over the box $V = [-a_x, a_x] \times [-a_y, a_y] \times [-a_z, a_z]$. The probability density of their location is hence

$$u(x, y, z) = \begin{cases} \dfrac{1}{8a_x a_y a_z}, & (x, y, z) \in V \\ 0, & \notin V. \end{cases} \tag{17}$$

We consider the evolution during one sampling interval of length Δt. Diffusive motion of the particle currently within the detection region is then described by convolving $u(x, y, z)$ with the isotropic Gaussian propagation in 3D

$$G(x, y, z) = G(x)G(y)G(z), \tag{18}$$

where

$$G(\cdot) = \frac{1}{\sqrt{2D\Delta t}} \phi\left(\frac{\cdot}{\sqrt{2D\Delta t}}\right). \tag{19}$$

We compute this convolution

$$\begin{aligned} h(x, y, z) = u * G(x, y, z) = \frac{1}{8a_x a_y a_z} &\int_{-a_x}^{a_x} G(x - x_0) dx_0 \\ &\times \int_{-a_y}^{a_y} G(y - y_0) dy_0 \int_{-a_z}^{a_z} G(z - z_0) dz_0, \end{aligned} \tag{20}$$

which simplifies to

$$\begin{aligned} h(x, y, z) = \frac{1}{8a_x a_y a_z} &\left[\Phi\left(\frac{x + a_x}{\sqrt{2D\Delta t}}\right) - \Phi\left(\frac{x - a_x}{\sqrt{2D\Delta t}}\right)\right] \\ &\times \left[\Phi\left(\frac{y + a_y}{\sqrt{2D\Delta t}}\right) - \Phi\left(\frac{y - a_y}{\sqrt{2D\Delta t}}\right)\right] \\ &\times \left[\Phi\left(\frac{z + a_z}{\sqrt{2D\Delta t}}\right) - \Phi\left(\frac{z - a_z}{\sqrt{2D\Delta t}}\right)\right]. \end{aligned} \tag{21}$$

Now, the probability of exiting the detection region is the integral of h outside of the detection region

$$\begin{aligned} P_{\text{exit}}(a_z) &= \iiint_{\mathbf{R}^3 \setminus V} h(x, y, z) dx dy dz \\ &= 1 - \iiint_{V} h(x, y, z) dx dy dz. \end{aligned} \tag{22}$$

This gives by straightforward computation

$$\begin{aligned} P_{\text{exit}}(a_z) = 1 - \frac{(2D\Delta t)^{3/2}}{8a_x a_y a_z} &\left\{\frac{2a_x}{\sqrt{2D\Delta t}} \left[2\Phi\left(\frac{2a_x}{\sqrt{2D\Delta t}}\right) - 1\right]\right. \\ &\left. + 2\phi\left(\frac{2a_x}{\sqrt{2D\Delta t}}\right) - 2\phi(0)\right\} \\ &\times \left\{\frac{2a_y}{\sqrt{2D\Delta t}} \left[2\Phi\left(\frac{2a_y}{\sqrt{2D\Delta t}}\right) - 1\right]\right. \end{aligned}$$

$$+ 2\phi\left(\frac{2a_y}{\sqrt{2D\Delta t}}\right) - 2\phi(0)\Bigg\}$$
$$\times\left\{\frac{2a_z}{\sqrt{2D\Delta t}}\left[2\Phi\left(\frac{2a_z}{\sqrt{2D\Delta t}}\right) - 1\right]\right.$$
$$\left. + 2\phi\left(\frac{2a_z}{\sqrt{2D\Delta t}}\right) - 2\phi(0)\right\}. \quad (23)$$

Appendix C: Stationary distribution

Because of diffusion equilibrium, the Markov chain has the stationary distribution as its initial distribution, and $\{X_n\}$ is hence a stationary process. There is a unique stationary distribution, since the chain is irreducible and all the states are nonnull recurrent. It follows from Grimmett & Stirzaker (2001), that the stationary distribution $\{\pi_k\}$ of the Markov chain described by the transition probabilities $\{p_{ij}\}$ is a Poisson distribution with parameter λ/μ, i.e.

$$P(X_n = k) = \pi_k = \frac{(\lambda/\mu)^k e^{-\lambda/\mu}}{k!} \quad (24)$$

for all $k \geq 0$ and all n.

Appendix D: Materials and methods

The experimental study was performed using a custom-built laser widefield epifluorescence microscope setup, based on a Nikon TE2000E microscope (Nikon BeLux, Brussels, Belgium) with a Nikon Plan Apochromat 60x NA1.20 water immersion objective lens. The sample was illuminated by a 100 mW Calypso 491 nm solid state laser (Cobolt, Solna, Sweden), from which the beam passes through an acousto-optic tunable filter (AA Optoelectronic, Orsay, France) which allows control of the intensity. The acousto-optic tunable filter can be synchronized with the charge-coupled device (CCD) camera, so that the sample only is illuminated during the light integrating phase which reduces photobleaching. The laser beam is directed through a 10° Light Shaping Diffuser (Physical Optics Corporation, Torrance, CA, U.S.A.), which in combination with an achromat lens in front of the microscope entrance provides widefield Kohler illumination at the sample. The fluorescence light coming from the sample is collected again by the objective lens and sent through the side port of the microscope towards the CCD camera. The fluorescence light is separated from the laser excitation light using a dichroic mirror and accompanying laser notch filter (AHF Analysentechnik, Tübingen, Germany). A pair of achromat lenses was placed between the CCD camera and the microscope side exit for an extra 1.5× magnification of the final image on the CCD chip. Since fast and sensitive image capture is required for single-particle imaging, an electron multiplying CCD camera was used (Cascade II:512; Roper Scientific, Tucson, AZ, U.S.A.). Image acquisition was performed using the Nikon Elements R imaging software. High-speed movies of individual particles diffusing in the suspension are acquired. Typically 5 μL of a water-particle solution was applied between a microscope slide and a cover glass with a double-sided adhesive sticker of 120 μm thickness (corresponding to $A_z = 60$ μm) in between (Secure-Seal Spacer; Molecular Probes, Leiden, The Netherlands). This provides for a 3D environment in which the particles can diffuse freely, while the sample is sufficiently thin to avoid convective drift. The microscope was always focused at least 20 μm from the cover glass to avoid deviations from free diffusion due to the presence of the cover slip. All experiments were carried out at 21°C and the full CCD chip was used, resulting in 512 by 512 pixel images. For the 0.2 μm particles, the physical pixel size and the sampling interval were 0.1329 μm and 38.2 ms, respectively. For the 0.5 μm particles, the physical pixel size and the sampling interval were 0.1329 μm and 58.0 ms, respectively. Forty videos for each dilution were acquired, all approximately 10 s long. The movies are analyzed using custom developed software to detect individual particles (see Braeckmans *et al.*, 2010a; Röding *et al.*, 2011).